Eur. Phys. J. D **45**, 477–483 (2007)
DOI: 10.1140/epjd/e2007-00257-7

THE EUROPEAN PHYSICAL JOURNAL D

Mass-selected Ag_3 clusters soft-landed onto MgO/Mo(100): femtosecond photoemission and first-principles simulations

T. Gleitsmann[1], M.E. Vaida[1], T.M. Bernhardt[1,a], V. Bonačić-Koutecký[2], C. Bürgel[2], A.E. Kuznetsov[2], and R. Mitrić[2]

[1] Institut für Oberflächenchemie und Katalyse, Universität Ulm, 89069 Ulm, Germany
[2] Institut für Chemie, Humboldt Universität zu Berlin, Brook-Taylor-Straße 2, 12489 Berlin, Germany

Received 31 January 2007 / Received in final form 18 May 2007
Published online 5 September 2007 –

Abstract. The electronic structure of supported mass-selected Ag_3 clusters is analyzed by joint femtosecond photoemission spectroscopy and ab initio theoretical investigations. A wide band gap insulating magnesia ultra-thin film on Mo(100) has been chosen as substrate in order to minimize the electronic interaction between metal clusters and support. After magnesia ultra-thin film preparation no photoemission from the molybdenum substrate is observed anymore, instead very weak two photon photoemission is detected possibly originating from surface or subsurface oxide defect states. Soft-landing deposition of 2% of atomic monolayer equivalents of Ag_3 clusters results in the disappearance also of the MgO two photon photoemission signal, while a strong single photon photoemission signal is detected from states located directly below the Fermi level. The theoretical study of structural, electronic and optical properties of Ag_3 at two model sites of MgO (100), the stoichiometric MgO(100) and an F_S-center defect, based on the DFT method and the embedded cluster model provides insight into the interactions between the cluster and the support which are responsible for the characteristic spectroscopic features.

PACS. 61.46.Bc Clusters – 36.40.Cg Electronic and magnetic properties of clusters – 79.60.-i Photoemission and photoelectron spectra – 68.47.Jn Clusters on oxide surfaces

1 Introduction

A great deal of experimental as well as theoretical efforts (see, e.g., [1]) have been devoted to elucidate the unique physics of matter in the size regime where 'each atom counts' [2] employing mass-selected silver clusters as prototype model systems in the gas phase and in few cases also on surfaces [3,4]. However, besides representing model systems to illustrate metal cluster size-effects, small clusters of silver are also strikingly unique as they exhibit molecule like luminescence properties with unprecedented efficiency when brought into a proper environment [5]. This surprising optical behavior was found for gas phase silver clusters in ultra-cold helium droplets and for deposited silver clusters in rare gas matrices [6], as well as for photolytically prepared silver clusters in silver oxide thin films [7,8]. On the basis of this photo-activated silver cluster luminescence new optical data storage media have been proposed and realized [7,9]. An understanding of the silver cluster optical and electronic properties on metal oxide supports is, however, just starting to emerge [10,11] and nothing is known so far about the photo-dynamics leading to such surprising optical properties.

In order to elucidate the hitherto unknown electronic structure of mass-selected silver clusters soft-landed onto a well-defined insulating metal oxide substrate we apply the technique of femtosecond two photon photoemission spectroscopy (fs-2PPS) employing a newly developed apparatus for cluster generation, mass-selection, soft-landing, as well as surface preparation and characterization [12]. Earlier fs-2PPS experiments on mass-selected silver clusters soft-landed onto a conducting graphite substrate demonstrated the influence of the cluster size on the energy distribution of the emitted photoelectrons and on the measured overall excitation decay [4]. In our experiments, a well-defined MgO(100) thin film grown in situ on a Mo(100) single crystal was chosen, because of the wide band gap of MgO even in films of only a few monolayers thickness [13], thus, minimizing the electronic coupling between metal clusters and surface with the aim to preserve the fascinating size dependent properties of small metal clusters. In the case of these ultra-thin films electron spectroscopic methods can still be applied without provoking charging effects [14].

2PPS investigations on metal oxides have considered so far TiO_2 [15,16], as well as large silver particles on MgO [17] and Al_2O_3 [18]. Large nanometer sized silver

[a] e-mail: thorsten.bernhardt@uni-ulm.de

particles and islands exhibit photoemission rather similar to metallic silver surfaces. The 2PP spectra obtained from bare semi-conducting TiO_2 crystal surfaces are characterized by electron emission from oxygen vacancy defects intentionally induced by annealing, electron or ion bombardment to achieve sufficient conductivity [15].

In this contribution we present a joint experimental and theoretical investigation of soft-landed Ag_3 clusters on ultra-thin MgO films. Cluster induced states near the Fermi level are identified by 2PPS. Ab initio calculations rule out Ag_3 clusters bound to stoichiometric MgO surface sites as origin of the observed photoemission and suggest bonding to defect sites instead. However, the calculations also show that a model defect site F_S-center also has a too high ionization energy to be in accord with the experimental findings.

2 Experimental setup and computational methods

The femtosecond photoemission investigations of monodisperse soft-landed silver clusters have been performed in a new ultra-high vacuum (UHV) cluster beam apparatus, which will be described in detail in a forthcoming publication [12]. The schematic layout of the experimental setup is outlined in Figure 1. The molybdenum single crystal with a diameter of 10 mm is mounted on a liquid nitrogen cryostat manipulator in the center of the photoemission chamber (base pressure $< 1 \times 10^{-10}$ mbar) and its temperature can be controlled by resistive heating between 90 and 1200 K. Cluster deposition and photoemission measurements are performed at 90 K. Initial crystal cleaning is performed by heating to 1600 K in $2{\times}10^{-7}$ mbar of oxygen and subsequent flash to 2000 K by direct electron bombardment [14,19]. The cleanliness and the quality of the Mo(100) surface as well as the thin film composition are routinely controlled by Auger electron spectroscopy (AES), electron energy loss spectroscopy (EELS) and low energy electron diffraction (LEED) [12]. In addition, the UHV photoemission chamber also comprises a quadrupole mass spectrometer for temperature programmed desorption (TPD) spectroscopy as well as several home-built evaporators for, e.g., magnesium and silver metal (see also Fig. 1).

Mass-selected silver clusters are generated by sputtering of silver-gold alloy targets with high energy Xe ion beams produced by a cold reflex discharge ion source (CORDIS [20]), subsequently thermalization is achieved in a helium filled radio-frequency (rf) quadrupole ion guide, and mass-selection via an rf quadrupole mass filter [21]. The mass-selected cluster ion beam is finally deflected by 90° and guided to the photoemission chamber via an Einzel lens arrangement and an rf octopole ion guide [12,22] (see Fig. 1). The kinetic energy spread of the cluster ion beam is determined directly before deposition to be less than 2 eV. This ensures soft-landing conditions with less than 1 eV per atom in the cluster when the appropriate retarding potential is applied to the substrate.

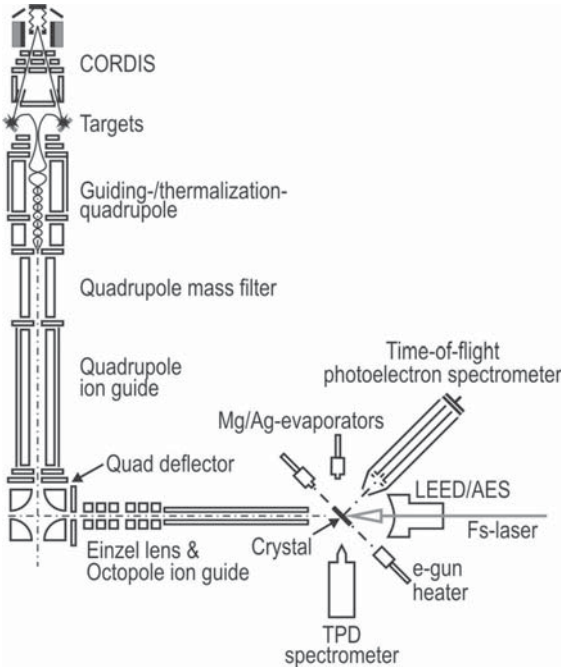

Fig. 1. Schematic layout of the cluster deposition and femtosecond photoemission experiment. See text for details.

The spatial width of the cluster beam impinging on the surface is about 5 mm. In the experiments presented here an Ag_3^+ cluster beam current of 120 pA resulted in deposition times of 30–40 min to obtain coverages of about 2% atomic monolayer (ML) equivalents of clusters on the magnesia surface.

The MgO(100) ultra-thin films are prepared according to the procedure reported in the literature by evaporation of magnesium metal (0.1 ML/min) in an atmosphere of $2{\times}10^{-7}$ mbar of oxygen [14,19]. During film preparation the Mo crystal is held at 600 K [23–25]. The films are subsequently annealed for 1 min at 1040 K. The obtained film thickness is typically 7–10 ML as determined by Auger electron spectroscopy [12].

Femtosecond photoemission spectra are measured with a home-built time-of-flight spectrometer consisting of a 0.6 m long double wall μ-metal tube. The femtosecond laser light is generated by a Ti:Sapphire oscillator (Kapteyn-Murnane-Laboratories), which is continuously pumped by a 6 W Spectra Physics Millennia Nd:YVO_4 laser. Pulse amplification is achieved with a Nd:YLF laser pumped Ti:Sapphire amplifier to yield 0.8 mJ, 40 fs, 804 nm center wavelength pulses at 1 kHz repetition rate. For the photoemission experiments presented here, the second harmonic (402 nm) of the fundamental laser emission wavelength has been used. The laser pulse energy was carefully adjusted between 1 and 70 nJ (irradiating a 2 mm^2 area on the substrate), in order to obtain comparable count rates avoiding spectral broadening due to space charge effects. Cross correlation measurements performed by detecting the integral two photon photoemission current from the molybdenum crystal surface directly inside the UHV chamber yield a typical pulse lengths of 80 fs.

The photoelectron spectrometer axis is oriented parallel to the surface normal and a bias of 3–5 V is typically applied to the sample. The laser beam incidence angle is 45° and the beam was p polarized in the experiments presented here.

In the calculations, the embedded cluster approach has been used for the description of the MgO support which is of ionic nature. The quantum mechanical treatment is restricted to $Mg_{13}O_{13}$ for stoichiometric MgO(100) and to $Mg_{13}O_{12}$ for the F_S-center. The array of point charges (PC) represented by $13\times13\times10$ describes the distant part of the electrostatic field of the support. In order to avoid strong polarization by positive PC's 16 Mg^{2+} cations have been introduced at the boundary of the model. This model is suitable for qualitative purposes. However, investigation of the size dependence of e.g. the ionization potential (IP) with increasing model size is out of scope of this work. The ground state structural and binding properties of Ag_3 at MgO support have been calculated using the density functional theory (DFT) method with gradient corrected Perdew-Burke-Ernzerhof (PBE) functional and an adequate basis set together with the 19 electron relativistic effective core potential (19e-RECP). For details cf. reference [11]. The structures of supported clusters were determined by full optimization of the cluster coordinates only since the relaxation of the neighboring support atoms did not change the binding energies significantly. The calculations of absorption spectra and photoelectron spectra and the optimization of the excited state geometries were performed employing time-dependent density functional theory (TDDFT) method with the PBE functional. For the silver atoms our 11e-RECP with the corresponding basis set was used since this ECP was derived for an accurate description of the excited states of silver clusters. The time-dependent DFT method usually describes adequately at least the lower energy excited states when compared with the more accurate methods for the free clusters. Since we focus on properties of low lying excited states the TDDFT can be used with confidence.

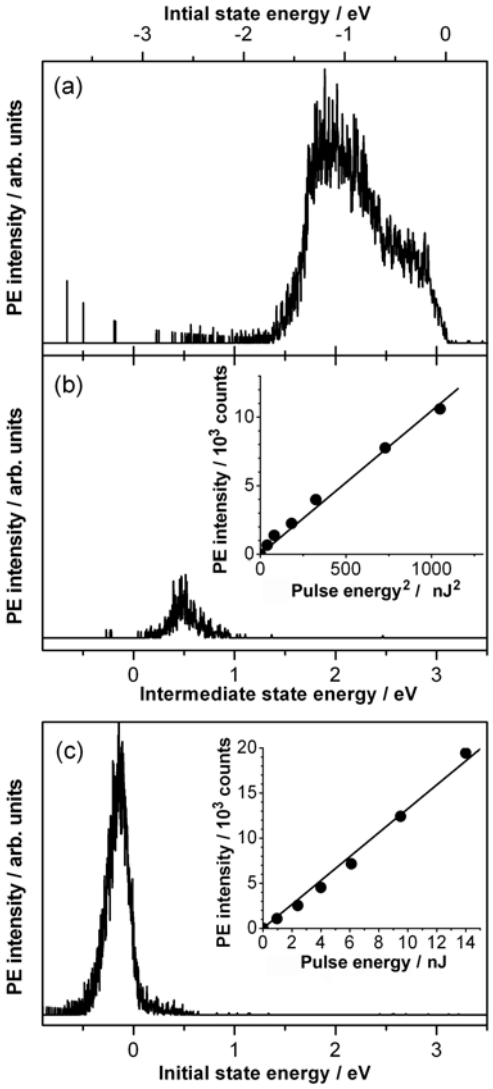

Fig. 2. Experimental femtosecond photoemission spectra obtained with 3.09 eV excitation energy (402 nm). (a) Clean Mo(100) surface (62 nJ laser pulse energy). (b) 8 ML MgO(100) film on Mo(100) (7 nJ laser pulse energy). The inset shows the quadratic power dependence of the photoemission signal. The bottom and top abscissae of (a) and (b) give the intermediate and initial state energies in the two photon excitation process with respect to the Fermi level. (c) 2% of atomic monolayer equivalents of Ag_3 clusters soft-landed onto MgO/Mo(100) (6 nJ laser pulse energy). The inset displays the power dependence of this photoemission signal. The linear behavior indicates a single photon excitation process. Therefore, for signal (c), the bottom abscissa displays the initial state energy in the one photon excitation process.

3 Results and discussion

In Figure 2a the 402 nm (3.09 eV) femtosecond two photon photoemission spectrum of the bare molybdenum (100) surface is displayed. This spectrum resembles the 2PP spectrum previously obtained from a polycrystalline molybdenum sample [27]. The corresponding two photon excitation mechanism is schematically depicted in Figure 3a. The first photon excites an electron from an initial state $|1\rangle$ within the molybdenum valence band to an intermediate state $|2\rangle$, which might correspond to an unoccupied real state resonance or a virtual state. The second photon then probes the population of state $|2\rangle$ by exciting an electron out of the intermediate state into the final state $|3\rangle$. If the final state energy is above the vacuum energy E_{vac}, the electron might leave the surface and its kinetic energy is measured with the time-of-flight electron energy analyzer. E_{vac} corresponds to the work function Φ, if the origin of the energy scale is set to the Fermi level E_F as it is the case in Figure 3, because of $\Phi = E_{vac}–E_F$. The high energy cut-off of the photoemission spectrum E_{max} represents electrons with their initial state energy at the Fermi level, $E_{max} = 2{\cdot}h\nu - \Phi = 2{\cdot}h\nu - E_{vac} - E_F$. It thus serves to define the Fermi level of the photoemission experiment which is particularly important for the investigation of the wide band gap magnesia ultra-thin films

without electronic states around the Fermi level and for the subsequent cluster deposition experiments. The low energy edge E_{min} of the Mo(100) 2PP spectrum in Figure 2a determines the work function Φ_{Mo} of the Mo(100) surface to be 4.5±0.1 eV ($\Phi_{\mathrm{Mo}} = 2{\cdot}h\nu - (E_{max} - E_{min})$). This value is in good agreement with the reported value of 4.53 eV [28].

No photoemission form molybdenum is detected anymore, if the metal substrate is covered with the magnesia ultra-thin film. Figure 2b shows that, instead, a new two photon photoemission signal is observed located around 0.5 eV intermediate state energy. The corresponding quadratic power dependence is displayed in the inset in Figure 2b. The width and the intensity of this signal changes slightly with each MgO preparation, however, a central location at 0.8±0.5 eV intermediate state energy and the general signal shape are reproducible for MgO films prepared at 600 K substrate temperature. A detailed investigation of the MgO/Mo(100) 2PP spectra obtained under different preparation conditions will be presented in a forthcoming contribution [24].

The two photon energy used in this experiment is not sufficient to release electrons from the oxygen $2p$ state-derived valence band of MgO, because it starts between 4 and 5 eV below E_F [13,29] and the reported work function of the MgO(100) surface amounts to $\Phi_{\mathrm{MgO}} = 2.7$ eV [30]. The photoemission signal from MgO displayed in Figure 2b originates form initial electronic states located not more than 2.8 eV below the Fermi level. These states within the band gap of MgO might be due to surface or subsurface defects. However, on the basis of the presented data the nature of this photoemission and the related initial states cannot be directly assigned to a specific defect type of MgO [31]. The energetic location of such states is tentatively indicated in the level schema of MgO depicted in Figure 3b. The low energy edge of this signal indicates a decrease in the work function $\Phi_{\mathrm{MgO/Mo}}$ of the MgO/Mo(100) system compared to the bare Mo(100) surface to 3.4–3.5 eV. This value is slightly larger than the literature value reported for the experimental work function of magnesia thin films (2.7 eV) [30]. Yet, this is not surprising as the work function of metal oxide surfaces is known to be extremely sensitive to the preparation procedure and the analytic method [29].

If 2% of atomic monolayer equivalents of Ag_3 clusters are soft-landed on the magnesia ultra-thin film, the experimental femtosecond photoemission spectrum changes again completely as can be seen from Figure 2c. A very intense photoemission signal is observed at small electron kinetic energies. Laser power dependent photoemission measurements clearly indicate that this signal is due to a single photon excitation as illustrated by the linear behavior of the respective graph displayed in the inset of Figure 2c. Therefore, it has to be concluded that the electron emission is due to a one photon transition from an occupied initial electronic state $|1\rangle$ to a final state $|3\rangle$. This is indicated schematically in the level schema in Figure 3c. The Ag_3 induced photoemission signal is therefore plotted in Figure 2c on an initial state energy axis corresponding to a single photon photoemission process. From this graph it is evident that the cluster induced signal originates from initial states $|1\rangle$ located at an energy $(E_1 - E_F) = -0.2$ directly below the Fermi level at $(E - E_F) = 0$. The low energy edge of the signal indicates a further decrease of the system work function to a value of about 2.7 eV. Besides a schematic representation of the location of the silver trimer cluster induced states, the decrease of the system work function is also included in the level schema in Figure 3c.

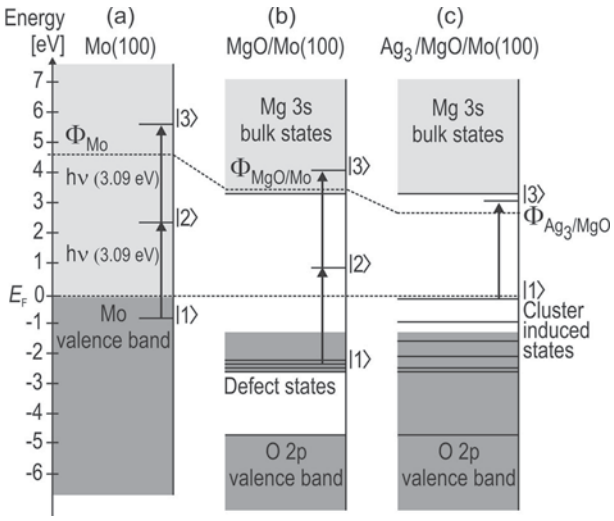

Fig. 3. Schematic level schemata for the different photoexcitation processes leading to the observed photoemission. All energies are plotted with respect to the Fermi level E_F. Two photon excitation processes involve the initial electronic state $|1\rangle$, the intermediate state $|2\rangle$, and the final state $|3\rangle$. (a) Two photon excitation of Mo(100). Depicted are the valence band (dark gray) and the conduction band (light gray) of molybdenum as well as the electronic work function Φ_{Mo} (dashed line). (b) Two photon excitation of MgO. The bulk band gap of MgO has been reported to be about 8 eV [13]. Depicted are the O $2p$ valence band at the bottom (dark gray) and the Mg $3s$ conduction band at the top of the band gap. Occupied electronic defect states located within the MgO band gap (dark grey area) between −2.8 eV and the Fermi level are assumed to be responsible for the observed photoemission signal from the magnesia ultra-thin film (Fig. 2b). No information about unoccupied electronic states within the band gap is available. The work function $\Phi_{\mathrm{MgO/Mo}}$ (dashed line) has decreased compared to the work function of Mo(100). (c) Soft-landing deposition of mass-selected Ag_3 clusters leads to a further decrease in the work function ($\Phi_{\mathrm{Ag_3/MgO}}$, dashed line). Single photon emission is observed (cf. Fig. 2c) from cluster induced electronic states located just below the Fermi level.

More detailed insight into the electronic structure of Ag_3 on different model sites of the MgO surface is gained from theoretical simulations. The calculations show that the silver trimer is perpendicularly bound to the stoichiometric site of MgO(100) and to the F_S-center as can be seen from the structure models in Figures 4a and 4b, respectively. In the former case two atoms are interacting with the surface and in the latter case interaction with

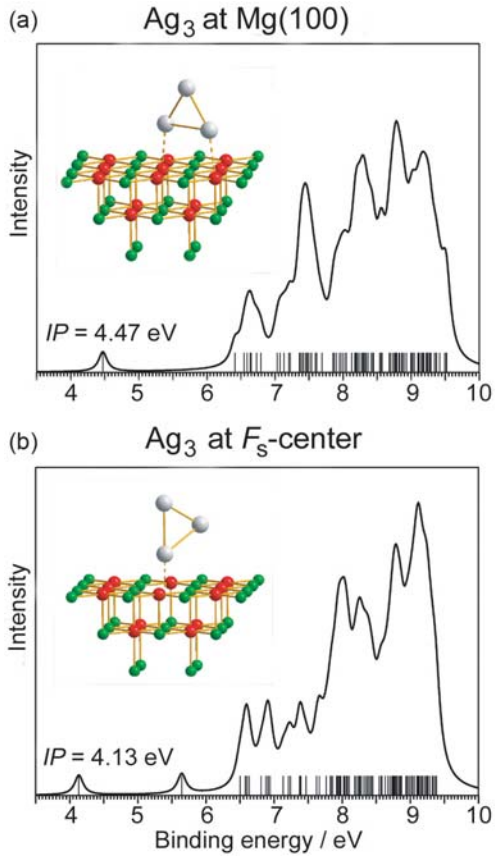

Fig. 4. (Color online) Calculated PES for (a) Ag_3 at MgO (100) and (b) Ag_3 at F_S-center. First peak corresponding to ionization potential of the system has been obtained using extended model for MgO (100) surface with $Mg_{98}O_{98}\left(Mg^{2+}\right)_{80}$ as QM part embedded in a $19 \times 19 \times 12$ point charge array.

a single atom is favored. The calculated binding energies are 1.04 eV and 2.4 eV, respectively. At the surface, the next isomer lies 0.115 eV higher in energy and assumes also trigonal shape with the tip pointing to the surface. In the case of the F_S-center, three isomers with trigonal Ag_3 unit and slightly different geometries lying within $\approx$ 0.05 eV have been found.

As detailed above, the experimental photoemission spectrum indicates an occupied electronic state due to soft-landed Ag_3 just below the Fermi level. The ionization potential IP of electrons occupying this state, i.e., the location of the state with respect to the vacuum level E_{vac}, is given by $\mathrm{IP} = (E_F - E_1) + \Phi_{\mathrm{MgO/Mo}} = 2.9$ eV. The theoretically determined one photon photoemission spectrum of Ag_3 at a stoichiometric MgO surface site is displayed in Figure 4a. The corresponding calculated IP for this stoichiometric surface site amounts to 4.47 eV. The comparison to the experimentally obtained value indicates that it is very unlikely that the observed photoemission (Fig. 2c) originates from Ag_3 clusters sitting on stoichiometric terrace sites. This is also supported by the experimental observation of the MgO emission at 0.5 eV intermediate state energy (cf. Fig. 2b) which indicates the presence of defect centers on the MgO surface. This emission almost disappears when Ag_3 clusters are deposited (Fig. 2c) pointing toward some interaction of the clusters with the MgO defect center sites.

The second model site simulated theoretically is the neutral oxygen vacancy on an MgO(100) terrace (F_S-center). The structural orientation of the silver cluster at this site and the calculated single photon photoemission spectrum are displayed in Figure 4b. The corresponding theoretical IP value is 4.13 eV an thus by 0.35 eV lower than the IP of Ag_3 at the stoichiometric surface. However, the higher theoretical IP value compared to the experimental IP indicates that the Ag_3 at an F_S-center site can also not be responsible for the experimental findings. Further work is in progress to characterize the nature of the Ag_3 binding sites on the MgO surface.

In order to provide more insight into the origin of the experimentally observed photoemission at 3.09 eV excitation energy, a comparison of the absorption spectra of free Ag_3 and Ag_3 at both MgO model sites is given in Figure 5. The lowest energy transitions for Ag_3 at the stoichiometric MgO(100) surface located at 1.8 eV is due to HOMO$\rightarrow$LUMO+2 excitation which can be characterized as a P$\rightarrow$D excitation. This transition is analogous to the transition of free Ag_3 which is located at 2.45 eV. The red shift for the supported Ag_3 is due to a strong polarization by the surface. In the case of Ag_3 at the F_S-center the lowest intense transition located at 1.8 eV is due to excitation also from HOMO$\rightarrow$LUMO+2 and is of P$\rightarrow$D nature. The HOMO orbital from which the excitation takes place is a combination of a cluster P-type orbital with appropriate P-type orbitals of the F_S-center. The red shift of this transition with respect to the free cluster is due to the interaction with the F_S-center. Although the lowest energy intense transitions of Ag_3 at both sites of MgO are located at the similar energy of 1.8 eV, the red shift with respect to the free cluster is due to different effects: polarization due to the surface versus F_S-center contribution. Optimization of the excited state geometry for both Ag_3 at stoichiometric MgO(100) surface and at the F_S-center defect gives rise to bound electronic states with minima close to absorption bands which in principle may be responsible for fluorescence.

Interestingly, there appears to be a pronounced difference of the absorption spectra of Ag_3 at the two model surface sites in the excitation energy range employed in the photoemission experiment. Whereas the calculated oscillator strength for Ag_3 at the stoichiometric surface site exhibits a minimum just above 3 eV (Fig. 5b), a pronounced maximum is calculated in this energy range for the case of Ag_3 at the F_S-center (Fig. 5c). The latter is due to the defect influence and characteristic not only for the terrace F_S-center. This result might be taken as a further qualitative support for the involvement of surface defects in the excitation mechanism leading to the observed photoemission. The presence of an intense transition at 1.8 eV ($\approx$700 nm) furthermore opens a perspective to carry out measurements of the lifetime of this state by the time resolved pump-probe photoemission experiment. The information about the lifetime of electronic states is crucial for

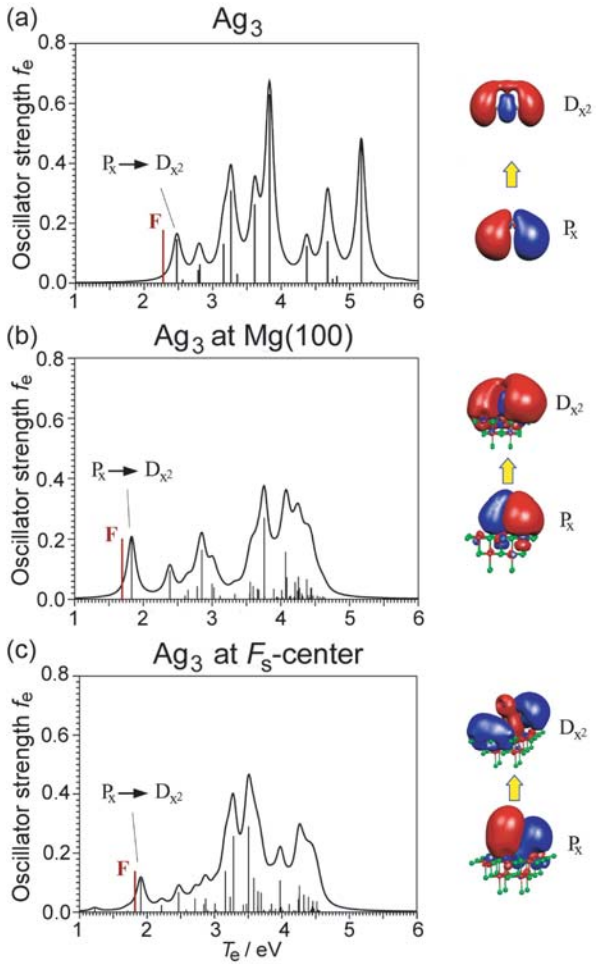

Fig. 5. (Color online) Comparison of calculated absorption spectra for (a) free Ag_3, (b) Ag_3 at stoichiometric MgO(100) and (c) Ag_3 at an F_S-center defect obtained for optimized structures. The nature of the characteristic electronic excitations involved in intense transitions are assigned and the corresponding orbitals are shown. The position of the fluorescence line (red line) obtained by optimizing the geometry of the excited state is labeled by F.

determining the efficiency of emissive centers in this model system.

In conclusion, our joint experimental and theoretical efforts elucidate the photoemission properties of silver trimer clusters soft-landed onto an ultra-thin film magnesia substrate. Femtosecond two photon photoemission is observed from defect centers on the bare magnesia substrate which disappears when silver clusters are deposited. Ag_3 gives rise to a strong one photon photoemission signal originating from electronic states located just below the Fermi level. The comparison to the theoretically obtained photoemission spectra of the silver cluster at two model surface sites excludes Ag_3 bound to the stoichiometric MgO(100) surface as cause for the experimental observations and supports the involvement of defects in the bonding of Ag_3. However, also the terrace F_S-center defect can be ruled out as bonding site for the silver clusters due to the considerably lower experimental ionization energy. Further experimental work is in progress to extend the investigations to different excitation energies and other silver cluster sizes supported by calculations of these clusters at various additional MgO defect sites.

MEV acknowledges the DAAD for a fellowship. TMB thanks Professor Ludger Wöste for the loan of laser equipment. Financial support by the Deutsche Forschungsgemeinschaft through priority program SPP1153 'Clusters at Surfaces' is gratefully acknowledged.

References

1. P. Fayet, L. Wöste, Surf. Sci. **156**, 135 (1985); G. Ganteför, M. Gausa, K.H. Meiwes-Broer, H.O. Lutz, J. Chem. Soc. Faraday Trans. **86**, 2483 (1990); J. Ho, K.M. Ervin, W.C. Lineberger, J. Chem. Phys. **93**, 6987 (1990); C. Jackschath, I. Rabin, W. Schulze, Ber. Bunsenges. Phys. Chem. **96**, 1200 (1992); K.J. Taylor, C.L. Pettiette-Hall, O. Cheshnovsky, R.E. Smalley, J. Chem. Phys. **96**, 3319 (1992); V. Bonačić-Koutecký, L. Cespiva, P. Fantucci, J. Pittner, J. Koutecký, J. Chem. Phys. **100**, 490 (1994); S. Wolf, G. Sommerer, S. Rutz, E. Schreiber, T. Leisner, L. Wöste, R.S. Berry, Phys. Rev. Lett. **74**, 4177 (1995); A. Fielicke, I. Rabin, G. Meijer, J. Phys. Chem. A **110**, 8060 (2006); X. Xing, R.M. Danell, I.L. Garzon, K. Michaelian, M.N. Blom, M.M. Burns, J.H. Parks, Phys. Rev. B **72**, 081405 (2005); P. Weis, T. Bierweiler, S. Gilb, M.M. Kappes, Chem. Phys. Lett. **355**, 355 (2002)
2. J. Jortner, Z. Phys. D **24**, 247 (1992); U. Landman, Int. J. Mod. Phys. B **6**, 3623 (1992); V. Bonačić-Koutecký, P. Fantucci, J. Koutecký, Chem. Rev. **91**, 1035 (1991)
3. K. Bromann, C. Felix, H. Brune, H. Harbich, R. Monot, J. Buttet, K. Kern, Surf. Sci. **377**, 1041 (1997); R. Schaub, H. Jödicke, F. Brunet, R. Monot, J. Buttet, W. Harbich, Phys. Rev. Lett. **86**, 3590 (2001); L. Benz, X. Tong, P. Kemper, Y. Lilach, A. Kolmakov, H. Metiu, M.T. Bowers, S.K. Buratto, J. Chem. Phys. **122**, 081102 (2005)
4. U. Busolt, E. Cottancin, H. Rohr, L. Socaciu, T. Leisner, L. Wöste, Eur. Phys. J. D **9**, 523 (1999); U. Busolt, E. Cottancin, H. Rohr, L. Socaciu, T. Leisner, L. Wöste, Appl. Phys. B **68**, 453 (1999); U. Busolt, E. Cottancin, L. Socaciu, H. Rohr, T. Leisner, L. Wöste, Eur. Phys. J. D **16**, 297 (2001)
5. F. Federmann, K. Hoffmann, N. Quaas, J.P. Toennies, Eur. Phys. J. D **9**, 11 (1999); T. Diederich, J. Tiggesbäumker, K.H. Meiwes-Broer, J. Chem. Phys. **116**, 3263 (2002); P. Radcliffe, A. Przystawik, T. Diederich, T. Döppner, J. Tiggesbäumker, K.H. Meiwes-Broer, Phys. Rev. Lett. **92**, 173403 (2004)
6. S. Fedrigo, W. Harbich, J. Buttet, Phys. Rev. B **47**, 10706 (1993); U. Kreibig, M. Vollmer, *Optical properties of metal clusters* (Springer, Berlin, 1995); W. Krasser, U. Kettler, P.S. Bechthold, Chem. Phys. Lett. **86**, 223 (1982); L. König, I. Rabin, W. Schulze, G. Ertl, Science **274**, 1353 (1996); C. Félix, C. Sieber, W. Harbich, J. Buttet, I. Rabin, W. Schulze, G. Ertl, Phys. Rev. Lett. **86**, 2992 (2001); W. Schulze, I. Rabin, G. Ertl, Chem. Phys. Chem **5**, 403 (2004)

7. L.A. Peyser, A.E. Vinson, A.P. Bartko, R.M. Dickson, Science **291**, 103 (2001); T. Gleitsmann, B. Stegemann, T.M. Bernhardt, Appl. Phys. Lett. **84**, 4050 (2004); T. Gleitsmann, T.M. Bernhardt, L. Wöste, Appl. Phys. A **82**, 125 (2006)
8. C.D. Geddes, A. Parfenov, I. Gryczynski, J.R. Lakowicz, J. Phys. Chem. B **107**, 9989 (2003); A. Maali, T. Cardinal, T. Treguer-Delapierre, Physica E **17**, 559 (2003)
9. B. Stegemann, T. Gleitsmann, T.M. Bernhardt, Verfahren zur optischen Datenspeicherung in Schichten aus Silberoxid mittels ultrakurzer Laserpulse (DE 10 2004 005 062 A1), Patentblatt des Deutschen Patent- und Markenamtes **125**, 21711 (2005)
10. C. Bürgel, R. Mitrić, V. Bonačić-Koutecký, Appl. Phys. A **82**, 117 (2006)
11. V. Bonačić-Koutecký, C. Bürgel, L. Kronik, A.E. Kuznetsov, R. Mitrić, Eur. J. Phys. D, submitted
12. M.E. Vaida, T. Gleitsmann, D. Popolan, S. Lang, G. Stibenz, B. Stegemann, L. Wöste, T.M. Bernhardt, in preparation
13. S. Schintke, S. Messerli, M. Pivetta, F. Patthey, L. Libioulle, M. Stengel, A. De Vita, W.-D. Schneider, Phys. Rev. Lett. **87**, 276801 (2001)
14. M.-C. Wu, J.S. Corneille, C.A. Estrada, J.-W. He, D.W. Goodman, Chem. Phys. Lett. **182**, 472 (1991); U. Heiz, F. Vanolli, L. Trento, W.-D. Schneider, Rev. Sci. Instrum. **68**, 1986 (1997)
15. K. Onda, B. Li, H. Petek, Phys. Rev. B **70**, 045415 (2004)
16. K. Onda, B. Li, J. Zhao, K.D. Jordan, J. Yang, H. Petek, Science **308**, 1154 (2005); J. Zhao, B. Li, K. Onda, M. Feng, H. Petek, Chem. Rev. **106**, 4402 (2006)
17. M. Aeschlimann, M. Bauer, S. Pawlik, R. Knorren, G. Bouzerar, K.H. Bennemann, Appl. Phys. A **71**, 485 (2000)
18. F. Evers, C. Rakete, K. Watanabe, D. Menzel, H.J. Freund, Surf. Sci. **593**, 43 (2005)
19. M.-C. Wu, J.S. Corneille, J.-W. He, C.A. Estrada, D.W. Goodman, J. Vac. Sci. Technol. A **10**, 1467 (1992)
20. R. Keller, F. Nöhmeier, P. Spädtke, M.H. Schönenberg, Vacuum **34**, 31 (1984)
21. T.M. Bernhardt, Int. J. Mass Spectrom. **243**, 1 (2005)
22. M. Vaida, *Design and Construction of a Low Energy Ion Guide System for Soft-Landing Experiments with Mass-Selected Metal Clusters,* Master-Thesis, Free University of Berlin, 2004
23. M. Sterrer, E. Fischbach, T. Risse, H.J. Freund, Phys. Rev. Lett. **94**, 186101 (2004)
24. T. Gleitsmann, M. Vaida, T.M. Bernhardt, in preparation
25. A. Sanchez, S. Abbet, U. Heiz, W.-D. Schneider, H. Häkkinen, R.N. Barnett, U. Landman, J. Phys. Chem. A **103**, 9573 (1999)
26. P.V. Sushko, A.L. Shluger, C.R.A. Catlow, Surf. Sci. **450**, 153 (2000)
27. A. Mönnich, J. Lange, M. Bauer, M. Aeschlimann, Phys. Rev. B **74**, 035102 (2006)
28. S. Berge, P.O. Gartland, B.J. Slagsvold, Surf. Sci. **43**, 275 (1974)
29. V.E. Henrich, P.A. Cox, *The Surface Science of Metal Oxides* (Cambridge University Press, Cambridge, 1996)
30. D. Ochs, W. Maus-Friedrichs, M. Brause, J. Günster, V. Kempter, V. Puchin, A. Shluger, L. Kantorovich, Surf. Sci. **365**, 557 (1996)
31. P.V. Sushko, J.L. Gavartin, A.L. Shluger, J. Phys. Chem. B **106**, 2269 (2002); G. Pacchioni, Chem. Phys. Chem. **4**, 1041 (2003); M. Sterrer, E. Fischbach, M. Heyde, N. Nilius, H.-P. Rust, T. Risse, H.J. Freund, J. Phys. Chem. B **110**, 8665 (2006); M. Sterrer, M. Heyde, M. Novicki, N. Nilius, T. Risse, H.-P. Rust, G. Pacchioni, H.J. Freund, J. Phys. Chem. B **110**, 46 (2006)